Improved broadband antireflection in Schottky-like junction of conformal Al-doped ZnO layer on chemically textured Si surfaces

C. P. Saini, A. Barman, M. Kumar, P. K. Sahoo, T. Som, and A. Kanjilal

---

Articles you may be interested in

Atomic layer deposition of Al-doped ZnO thin films
J. Vac. Sci. Technol. A 31, 01A109 (2013); 10.1116/1.4757764

Growth morphology and electrical/optical properties of Al-doped ZnO thin films grown by atomic layer deposition
J. Vac. Sci. Technol. A 30, 021202 (2012); 10.1116/1.3687939

Light confinement-induced antireflection of ZnO nanocones
Appl. Phys. Lett. 99, 153113 (2011); 10.1063/1.3651751

Synthesis and characterization of ZnO thin film grown by electron beam evaporation
J. Appl. Phys. 99, 123105 (2006); 10.1063/1.2204333

Highly textured and conductive undoped ZnO film using hydrogen post-treatment
Appl. Phys. Lett. 70, 3516 (1997); 10.1063/1.119218

Improved broadband antireflection in Schottky-like junction of conformal Al-doped ZnO layer on chemically textured Si surfaces

C. P. Saini,[1] A. Barman,[1] M. Kumar,[2] P. K. Sahoo,[3] T. Som,[2] and A. Kanjilal[1,a)]

[1]*Department of Physics, School of Natural Sciences, Shiv Nadar University, Gautam Budh Nagar, Uttar Pradesh 201 314, India*
[2]*SUNAG Laboratory, Institute of Physics, Bhubaneswar 751 005, Odisha, India*
[3]*School of Physical Sciences, National Institute of Science Education and Research, Bhubaneswar 751 005, Odisha, India*

Chemically textured Si with improved absorption in the complete range of solar spectrum is investigated by ultraviolet/visible/near-infrared (UV/Vis/NIR) spectroscopy, showing an average specular reflectance of ~0.4% in the wavelength of 500–3000 nm. The pyramidal structures on such solar-blind Si can reduce the reflectance further below 0.1% in the UV region by conformal growth of granular Al-doped ZnO (AZO) films. X-ray diffraction analyses suggest the growth of polycrystalline AZO on faceted-Si. Moreover, marginal increase in electrical conductivity of AZO is found on textured surfaces, whereas rise in leakage current in Schottky-like Ag/AZO/Si/Ag heterostructure devices is noticed with increasing Si surface area. © 2014 AIP Publishing LLC.
[http://dx.doi.org/10.1063/1.4896340]

The progress of crystalline Si (*c*-Si) solar cells is hindered by the surface reflection loss, especially for polished flat-Si with high specular reflectance of about 30%–40%.[1] Although an optically transparent quarter wavelength ($\lambda/4$) thick SiO_x, TiO_x, or Si_xN_y layer is conventionally employed as an antireflection coating (ARC),[2] such a single layer is applicable only for a limited wavelength of the solar spectrum and also for specific incidence angles.[3] Therefore, it requires a multilayer structure with intermediate or gradient refractive indices for (a) increasing spectral width[4] and (b) reducing reflection (up to ~18% till date).[5] In this context, subwavelength biomimetic textures can not only give an alternative approach to improve antireflection (AR) property using multiple reflection[2,6] but also offer additional trapping/absorption of solar spectrum by diffuse scattering[7] and/or mode coupling.[8] As AR property is known to be strongly influenced by the shape, distribution, and aspect ratio of the faceted structures,[9,10] controlled preparation of textured surfaces is the key to minimize the reflection loss. Moreover, the success of Si photovoltaic (PV) solar cells depends on the processing cost. We should note here that the chemical etching is known to be easy and inexpensive approach for producing both front and rear textured surfaces, and therefore imperative for Lambertian light trapping.[7] However, precise control over chemical etching is still required to bring the reflection down below 5%–12% to compete with other contemporary techniques such as reactive-ion etching,[2] laser ablation,[11] and ion-beam sputtering.[12] It is even challenging to suppress it below 1% for the complete solar spectrum.[13]

Since the present textured Si surfaces are capable of reducing reflection only in the visible range,[2] it is therefore essential to develop solar-blind Si surfaces with lowest possible reflectance both in the ultraviolet (UV) and near-infrared (NIR) regions. Moreover, metal-like electrical conductivity of the transparent conducting layer on textured Si will be advantageous to overcome the drawbacks of ARC, which involves increased area of metal contact for charge collection.[14] In this respect, metal-oxides are promising for having broadband transparency with strong absorption capability in the UV region, though electrical conductivity can be improved by doping impurities. For instance, large bandgap (~3.4 eV) ZnO[15] is favorable for UV absorption, while Al-doping increases the electrical conductivity.[16] The application of this transparent conducting oxide (TCO) in PV technology, however, demands conformal growth of Al-doped ZnO (AZO) on textured-Si surfaces.[17,18]

In this letter, we show the efficacy of chemically etched pyramidal structures on Si to bring the average specular reflectance down to ~0.4% in the wavelength of 500–3000 nm, and even below 0.1% in the UV region by conformal growth of AZO layer. We further show how the Ohmic behavior of AZO is slightly increased on textured Si, and leakage current is enhanced in Ag/AZO/Si/Ag heterostructure devices.

To evaluate this, a 500 μm thick *p*-type Si(100) wafer was diced into several pieces (area ~1 × 1 cm^2). Prior to chemical texturing, saw-damage-removal (SDR) process was carried out. Here, ultrasonically cleaned Si substrates were etched in a 30 wt. % NaOH solution (in H_2O) at 75 °C for 3 min during which both top and rear surfaces were cleaned by removal of 5–7 μm thick Si from either surface. Afterwards, controlled chemical texturing was executed at 70 °C for 40 min in 3 wt. % NaOH solution in the presence of 10% isopropyl-alcohol (IPA). Chemically etched Si substrates were further immersed in 20% HCl for 2 min, followed by rinsing in deionized (DI) water to remove Na residues. Finally, they were cleaned in 10% HF for 20 s not only for removing native SiO_x but also for neutralizing the remaining chemicals. Chemically etched Si surfaces were eventually rinsed in DI water and dried by nitrogen blow. The etching process was optimized based on the UV/Visible/NIR (UV/Vis/NIR) results as will be discussed in the following.

a)Electronic mail: aloke.kanjilal@snu.edu.in

Followed by chemical etching, using the deposition condition of AZO on flat-Si,[19] a 75 nm thick AZO layer was grown on textured Si at room temperature (RT) by pulsed dc magnetron sputtering method with a base pressure of $\sim 2 \times 10^{-7}$ mbar. Commercially available 99.99% pure AZO target composed of 98 wt. % ZnO and 2 wt. % Al was used for AZO deposition. Highly pure (99.999%) Ar gas was injected into the chamber at a rate of 30 sccm during AZO deposition, giving a working pressure of $\sim 5 \times 10^{-3}$ mbar. The target-to-substrate distance was maintained at ~ 8 cm, while an input dc power of 100 W was applied to the AZO target. In addition, the substrate was rotated with a speed of 3 rpm to have a uniform film thickness.

The surface morphologies of the textured Si substrates before and after AZO deposition were examined by scanning electron microscopy, SEM (Carl Zeiss) in both plan-view and cross-sectional geometries. Crystallinity and phase were diagnosed by x-ray diffraction, XRD (Bruker, D8-Discover) using a Cu-K_α radiation ($\lambda = 0.154$ nm). Moreover, specular reflectance was examined by UV/Vis/NIR spectrophotometer (Shimadzu, 3101PC) using unpolarized light. The electrical transport measurements of the AZO layer and Ag/AZO/Si/Ag heterostructure devices were carried out independently by a source-meter (Keithley 2410).

Typical plan-view and cross-sectional SEM images of chemically etched Si surfaces are exhibited in Figs. 1(a) and 1(b), respectively, showing random distribution of pyramidal structures. We should note here that the {111} facets are formed because of high etching rate of (100) plane with respect to (111) plane (see Ref. 20 and references therein). Close inspection of Fig. 1(a) shows: (i) protrusions jutted out from the {111} facets of the sidewalls as well as from the bottom (indicated by dashed rectangles) and (ii) cluster of small pyramids (pointed out by dashed circle). This can be seen clearly in cross-sectional SEM (XSEM) where one of such features is indicated by a downward arrow. The average height (d) and distance between two consecutive pyramids (a) are found to be controlled by etching time and temperature. Since the aspect ratio of d and a is known to influence the reflection property, the present focus was to maintain the

corresponding values on the order of 2.5 and 2 μm to minimize the reflection loss.[9] In fact, except bigger pyramids with height in the range of 4–6 μm (like in conventional *c*-Si solar cells),[10] both d and a for remaining faceted structures are found to be on the order of $\sim$2.5–3 μm and 2–2.5 μm, respectively [Fig. 1(b)]. Here, IPA plays a crucial role in the evolution of chemically etched pyramids on Si.[21]

The conformal growth of a 75 nm thick AZO layer on faceted Si is evident in Fig. 1(c). Clearly, the AZO layer maintains the protrusions on the {111} facets as marked by an arrow, while magnified XSEM image delimitates the formation of irregular shaped 25–30 nm grains [Fig. 1(d)]. The evolution of these grains can be elucidated in the light of Volmer-Weber type of nucleation of adatoms on the {111} facets to reduce the surface free energy.[22]

As expected from Ref. 19, grains are also formed on flat Si, Si_{Flat}, surfaces (not shown). Therefore, the structure of AZO on textured Si is compared with the one grown on Si_{Flat} by XRD in the 2θ range of 30°–75°, where θ is the Bragg's angle (Fig. 2). In fact, on Si_{Flat}, a single diffraction peak of AZO is found to be originated at $\sim$34.5° in conjunction with relatively strong reflections from the (200) and (400) planes of underneath Si substrate at $\sim$33.4° and $\sim$69.5°, respectively. Indeed, the AZO peak is assigned to the reflection from the (002) plane, indicating preferential orientation of grains along *c*-axis.[18] On the other hand, the (002) peak of AZO is completely disappeared on textured Si, instead it leads to the evolution of (101), (102), and (103) peaks at $\sim$36.6°, 47.9°, and 62.9°, respectively.

Careful analysis further suggests that the (101) peak intensity dominates over (102) and (103) peaks. This can be explained in the framework of preferential growth of AZO along *c*-axis on the {111} facets of Si pyramids. In this model, the (002) plane of AZO is rotated by 45° with respect to the one observed on Si_{Flat}. Based on this concept, Bragg's law cannot be fulfilled for the (002) plane on textured Si within the projected range of 2θ. On the other hand, the incident x-rays can reflect from the (101) plane which is situated at an angle of 45° from the (002) plane, in good agreement with the observed results (Fig. 2). Although the Bragg reflection is allowed for (102) and (103) planes, their relatively
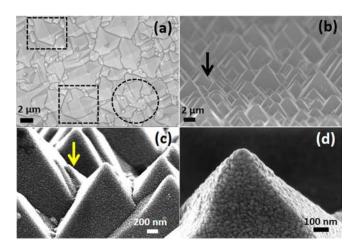

FIG. 1. SEM images of Si textured substrate in (a) horizontal and (b) cross-sectional geometries. The cross-sectional SEM image of AZO layer on textured Si surface is shown in (c), while (d) shows the magnified view of such a pyramid.
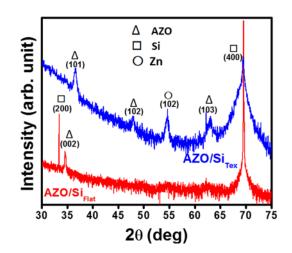

FIG. 2. XRD patterns of AZO layers on textured Si (blue curve) and pristine Si (red curve). The detected Si, AZO, and Zn peaks are indicated by open squares (□), open triangles (△), and open circle (○), respectively.

weak peak intensities are likely to be associated with low scattering cross-section. Another peak which is detected at $\sim$54.6° is attributed to a reflection from Zn grains that seem to be formed via segregation of Zn atoms during AZO deposition. These grains are most possibly residing at the apex of the Si facets as was reported recently by Basu *et al.*[18] Using the (102) peak, the average size of crystalline Zn grains was determined to be 16 ± 2 nm by Scherer formula:[19] $D = 0.9\lambda / \beta\cos\theta$ where D is the crystal size, β is the full width at half maximum, and λ is the x-ray wavelength.

The key finding is the minimum reflection loss from textured Si in the visible and NIR regions, while the UV range is suppressed by conformal growth of AZO layer. The specular reflectance (R) is, however, correlated with absorbance ($A = 1 - T - R$) that can be improved by subsequent reduction of R, provided there is no transmission (T) loss during UV/Vis/NIR measurements. Figure 3(a) shows typical variation of R as a function of wavelength in the range of 300–3000 nm for an optimized sample, while the corresponding absorbance spectrum is displayed in Fig. 3(b). The insets of Figs. 3(a) and 3(b) represent the magnified view of the reflectance and absorbance spectra with and without AZO layer on textured Si. As can be seen, the average value of R can reach to $\sim$0.4% within 500–3000 nm in absence of AZO, while this goes further down together with a significant drop in the UV region ($\sim$0.1%) by depositing AZO layer. As mentioned above, the observed reflectance/absorbance can be evaluated in the light of aspect ratio (d/a) of submicron pyramids. Here, the large aspect ratio for $d > a$ provides a hefty surface area like in nanowires, which in turn enhances surface recombination.[13] Therefore, in order to achieve minimum R with least surface recombination of charge carriers, d/a ratio should be within 1–2.[9] This is in good agreement with our SEM results (Fig. 1). It is worthwhile to note that R plays an important role in solar devices as the internal quantum efficiency, IQE = EQE/(1 − R), where EQE is the external quantum efficiency.[20]

While the aspect ratio d/a of the pyramids in the front surface improves the AR property, faceted structures in the rear surface assist in improving light trapping by maximizing photon absorption via internal scattering in the NIR region and by reducing surface recombination.[22] Although these microscale pyramids exhibit an excellent AR for broad band solar spectrum, they still show considerably high reflectance around 400–500 nm due to the limitation of geometrical optics effect.[23] This can be overcome by introducing AZO on textured Si as it provides a strong absorption edge in this region and thus improves light trapping property. However, the present results show the formation of AZO grains on textured Si [Figs. 1(c) and 1(d)], which eventually leads to further suppression of R due to the increase in Si surface area [illustrated schematically in the inset of Fig. 3(b)]. Here the ray diagram shows how the light absorption is boosted by increasing surface area due to anisotropic texturing of Si surfaces where the lower refractive index of AZO grain boundaries with respect to the grains can also participate in light absorption via internal reflection.[24] In fact, graded refractive index is advantageous for refining light absorption[5] where R of a material strongly depends on its reflective index (n):[25] $n = \left(\frac{1+R}{1-R}\right) + \sqrt{\frac{4R}{(1-R)^2} - k^2}$. Here, k ($= \alpha\lambda/4\pi$) is the extinction coefficient. In this case, the reflective index of AZO ($n \sim 2.2$–1.8 for $\lambda = 300$–800 nm)[26] between air ($n \sim 1$) and c-Si ($n \sim 3.4$) can engineer a graded reflective index for suppressing the Fresnel reflection over a broad range of solar spectrum. During UV/Vis/NIR measurements, identical spectra have also been observed in all azimuthal angles, confirming the isotropic nature of AR property. Such intriguing broadband AR property in the wavelength of 300–3000 nm is promising over other competitive techniques that include ion-beam etching (proving a minimum reflectance of $\sim$2.5% up to 1000 nm)[17] and ion-beam erosion (showing AZO thickness-dependent tunable AR window in association with wavelength-specific local reflectance minima below 1%).[18]
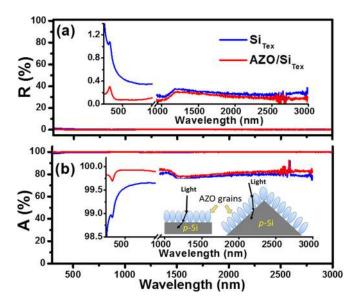

FIG. 3. Reflectance (R) and absorbance (A) spectra of textured Si without AZO (blue curves) and with AZO (red curves) are shown in (a) and (b), respectively. The corresponding magnified spectra are highlighted in the insets of (a) and (b). The formation of AZO grains on flat and textured Si surfaces is presented schematically in the inset of (b), while ray diagram indicates the light trapping processes in both AZO layers and Si substrates.
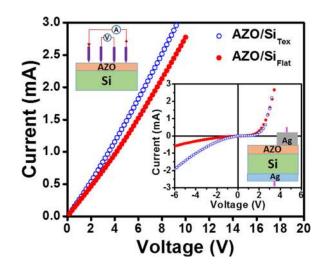

FIG. 4. *I-V* characteristics of AZO layer on flat Si (filled circles) and textured Si (open circles) surfaces determined by four-probe technique (shown schematically in the left inset, top corner). *I-V* characteristics of the AZO/Si heterostructure devices (schematically shown in the right inset, lower corner) with (open circles) and without (filled circles) texturing on Si surfaces showing the rectifying property.

In order to investigate the effect on electrical conductivity of the AZO layer on textured Si, current-voltage (*I-V*) characteristics were recorded at RT in dark condition by four-probe technique on both textured and flat Si surfaces (Fig. 4). For measuring *I-V* characteristics, circular electrical contacts (with an average diameter of 2 mm) were prepared on AZO layer by Ag paste. One can see that the slope is increased marginally on textured Si where the linear profiles in both (flat and textured Si) cases show a metallic behavior of AZO. The reason behind the observed increase in Ohmic behavior is not clear yet, though we believe that it could be due to the rise in average aerial density of AZO grains with increasing surface area of textured Si; this in turn reduces the scattering loss of charge carriers at grain boundaries, and as a result increases the mean free path of electrons (see Ref. 19 and references therein). This may further be supported by the improving collection of photogenerated minority carriers by minimizing recombination loss[27] via decreasing the ratio of minority carrier collection length to optical absorption depth.[28] In the present experiments, ZnO is most likely degenerately doped in the presence of 2 at. % Al where the involved carrier concentration ($\sim 5 \times 10^{20}$ cm^{-3}) moves the Fermi level into the conduction band.[29] Under this circumstance, the dopants are very easily ionized without any external thermal energy and eventually show a metallic behavior with high carrier mobility.[29] In comparison to flat-Si, surface resistivity of AZO film on textured Si slightly decreases from 0.13 to 0.1 Ω-cm. Note that resistivity depends on the thickness of AZO layer.[19] Meanwhile, RT diode characteristics of the Schottky-like Ag/AZO/Si/Ag heterostructure devices (inset, right corner) show the rectifying behavior with a minute change in turn-on potential on texture Si, signifying negligible variation in potential barrier at the AZO/Si interface.[19] On the other hand, it shows a clear increase in leakage current on textured Si due to the increase in junction area. This can be explained in the framework of increasing traps at the AZO/Si interface,[30,31] and thus it requires a buffer layer as the one proposed in Ref. 32.

In conclusion, we report a chemical etching process of Si that gives an average specular reflectance of ~0.4% in the wavelength range of 500–3000 nm due to the formation pyramidal-shaped faceted structure. This can go further down, especially in the UV region up to ~0.1%, by conformal growth of AZO layer. These intriguing phenomena have been discussed in the light of size and aspect ratio of Si pyramids in conjunction with active participation of AZO in absorbing UV light. This is further anticipated by graded refractive indices at the AZO/Si interface with increasing Si surface area. Moreover, minor increase in metallic behavior of AZO on textured Si proves its potential to be used as a TCO layer, whereas the observed increase in leakage current in Schottky-like Ag/AZO/Si/Ag heterostructure devices due to the upsurge of traps on faceted Si needs to be inhibited for various applications, especially for solar cells.

[1]S. Strehlke, S. Bastide, and C. Lévy-Clément, Sol. Energy Mater. Sol. Cells **58**, 399 (1999).

[2]K. N. Nguyen, P. Basset, F. Marty, Y. Leprince-Wang, and T. Bourouina, J. Appl. Phys. **113**, 194903 (2013).

[3]M. A. Green, *Silicon Solar Cells: Advanced Principles and Practice* (NSW Bridge Printery, Sydney, 1995).

[4]L. Ye, Y. Zhang, X. Zhang, T. Hu, R. Ji, B. Ding, and B. Jiang, Sol. Energy Mater. Sol. Cells **111**, 160 (2013).

[5]S. Chhajed, M. F. Schubert, J. K. Kim, and E. F. Schubert, Appl. Phys. Lett. **93**, 251108 (2008).

[6]K. X. Wang, Z. Yu, V. Liu, Y. Cui, and S. Fan, Nano Lett. **12**, 1616 (2012).

[7]M. A. Green, Prog. Photovoltaics Res. Appl. **10**, 235 (2002); M. L. Brongersma, Y. Cui, and S. Fan, Nat. Mater. **13**, 451 (2014).

[8]G. Gomard, E. Drouard, X. Letartre, X. Meng, A. Kaminski, A. Fave, M. Lemiti, E. Garcia-Caurel, and C. Seassal, J. Appl. Phys. **108**, 123102 (2010); A. Lin, Y.-K. Zhong, and S.-M. Fu, *ibid*. **114**, 233104 (2013).

[9]H. Sai, Y. Kanamori, K. Arafune, Y. Ohshita, and M. Yamaguchi, Prog. Photovoltaics Res. Appl. **15**, 415 (2007).

[10]H. Kim, S. Park, B. Kang, S. Kim, S. J. Tark, D. Kim, and S. S. Dahiwale, Appl. Surf. Sci. **284**, 133 (2013).

[11]D. Riabinina, C. Durand, M. Chaker, and F. Rosei, Appl. Phys. Lett. **88**, 073105 (2006).

[12]K. Zhang, O. Bobes, and H. Hofsass, Nanotechnology **25**, 085301 (2014).

[13]S. Chattopadhyay, Y. F. Huang, Y. J. Jen, A. Ganguly, K. H. Chen, and L. C. Chen, Mater. Sci. Eng. Rep. **69**, 1 (2010).

[14]N. A. Estrich, D. H. Hook, A. N. Smith, J. T. Leonard, B. Laughlin, and J.-P. Maria, J. Appl. Phys. **113**, 233703 (2013).

[15]J. G. Reynolds, C. L. Reynolds, Jr., A. Mohanta, J. F. Muth, J. E. Rowe, H. O. Everitt, and D. E. Aspnes, Appl. Phys. Lett. **102**, 152114 (2013).

[16]J. G. Lu, Z. Z. Ye, Y. J. Zeng, L. P. Zhu, L. Wang, J. Yuan, B. H. Zhao, and Q. L. Liang, J. Appl. Phys. **100**, 073714 (2006).

[17]M. Otto, M. Kroll, T. Kasebier, S.-Mo. Lee, M. Putkonen, R. Salzer, P. T. Miclea, and R. B. Wehrspohn, Adv. Mater. **22**, 5035 (2010).

[18]T. Basu, M. Kumar, P. K. Sahoo, A. Kanjilal, and T. Som, Nanoscale Res. Lett. **9**, 192 (2014).

[19]M. Kumar, A. Kanjilal, and T. Som, AIP Adv. **3**, 092126 (2013).

[20]M. Hong, G. D. Yuan, Y. Peng, H. Y. Chen, Y. Zhang, Z. Q. Liu, J. X. Wang, B. Cai, Y. M. Zhu, and Y. Chen, Appl. Phys. Lett. **104**, 253902 (2014).

[21]P. Papet, O. Nichiporuk, A. Kaminski, Y. Rozier, J. Kraiem, J. F. Lelievre, A. Chaumartin, A. Fave, and M. Lemiti, Sol. Energy Mater. Sol. Cells **90**, 2319 (2006).

[22]S.-W. Kim, S. Fujita, and S. Fujita, Jpn. J. Appl. Phys., Part 2 **41**, L543 (2002).

[23]R. B. Stephens and G. D. Cody, Thin Solid Films **45**, 19 (1977).

[24]H. C. Ong, J. Y. Dai, K. C. Hung, Y. C. Chan, R. P. H. Chan, and S. T. Ho, Appl. Phys. Lett. **77**, 1484 (2000).

[25]*Optical Properties of Solids*, edited by F. Abeles (North-Holland Publishing Company, London, 1972).

[26]K. Qiu, Y. Zhao, Y. Gao, X. Liu, S. Cao, J. Tang, Y. Zhang, B. Feng, and X. Xu, Appl. Phys. Lett. **104**, 081109 (2014).

[27]M. Gharghi, E. Fathi, B. Kante, S. Sivoththaman, and X. Zhang, Nano Lett. **12**, 6278 (2012).

[28]S. W. Boettcher, J. M. Spurgeon, M. C. Putnam, E. L. Warren, D. B. Turner-Evans, M. D. Kelzenberg, J. R. Maiolo, H. A. Atwater, and N. S. Lewis, Science **327**, 185 (2010).

[29]K. Ellmer and R. Mientus, Thin Solid Films **516**, 5829 (2008).

[30]*Transparent Conductive Zinc Oxide: Basics and Applications in Thin Film Solar Cells*, edited by K. Ellmer, A. Klein, and B. Rech (Springer, Berlin, 2007).

[31]H.-D. Um, S. A. Moiz, K.-T. Park, J.-Y. Jung, S.-W. Jee, C. H. Ahn, D. C. Kim, H. K. Cho, D.-W. Kim, and J.-H. Lee, Appl. Phys. Lett. **98**, 033102 (2011).

[32]A. K. Pradhan, T. Holloway, R. Mundle, H. Dondapati, and M. Bahoura, Appl. Phys. Lett. **100**, 061127 (2012).